Characteristic energies, transition temperatures, and switching effects in clean S|N|S graphene nanostructures

Klaus Halterman,[1,*] Oriol T. Valls,[2,†] and Mohammad Alidoust[3,‡]

[1]*Michelson Lab, Physics Division, Naval Air Warfare Center, China Lake, California 93555, USA*

[2]*School of Physics and Astronomy, University of Minnesota, Minneapolis, Minnesota 55455, USA*

[3]*Department of Physics, Norwegian University of Science and Technology, N-7491 Trondheim, Norway*

(Received 20 May 2011; revised manuscript received 11 July 2011; published 19 August 2011)

We study proximity effects in clean nanoscale superconductor–normal-metal–superconductor (S|N|S) graphene heterostructures using a self-consistent numerical solution to the continuum Dirac Bogoliubov–de Gennes (DBdG) equations. We obtain results for the pair amplitude and the local density of states (DOS) as a function of doping and of the geometrical parameters determining the width of the structures. The superconducting correlations are found to penetrate the normal graphene layers even when there is extreme mismatch in the normal and superconducting doping levels, where specular Andreev reflection dominates. The local DOS exhibits peculiar features, which we discuss, arising from the Dirac cone dispersion relation and from the interplay between the superconducting and Thouless energy scales. The corresponding characteristic energies emerge in the form of resonant peaks in the local DOS, which depend strongly on the doping level, as does the energy gap, which declines sharply as the relative difference in doping between the S and N regions is reduced. We also linearize the DBdG equations and develop an essentially analytical method that determines the critical temperature T_c of a S|N|S nanostructure self-consistently. We find that for S regions that occupy a fraction of the coherence length, T_c can undergo substantial variations as a function of the relative doping. At finite temperatures and by manipulating the doping levels, the self-consistent pair amplitudes reveal dramatic transitions between a superconducting and resistive normal state of the structure. Such behavior suggests the possibility of using the proposed system as a carbon-based superconducting switch, turning superconductivity on or off by tuning the relative doping levels.

DOI: 10.1103/PhysRevB.84.064509 PACS number(s): 74.45.+c, 71.10.Pm, 73.23.Ad

I. INTRODUCTION

The successful development of methods to create large samples of graphene,[1,2] has been followed by recent efforts to exploit its high electron mobility[3,4] and the peculiar band structure[5] associated with its two dimensionality. A number of graphene-based devices have been subsequently proposed,[6] including field-effect transistors, quantum information storage systems, optoelectronic devices, and nanoscale superconducting systems. In particular, the observation of superconductivity in graphene,[7–11] either through doping or by means of superconducting contacts, has fueled research activity involving proximity effects in normal (N) and superconductor (S) graphene regions that are in close electrical contact.[12] Indeed, the presence of superconducting correlations in graphene is remarkable considering that undoped graphene in isolation is inherently nonsuperconducting even at low temperatures. Striking evidence of the peculiarities of superconductivity in graphene was the observation of a Josephson supercurrent induced by two superconducting electrodes in close contact with the graphene.[8] The tunneling conductance of a junction consisting of an insulating barrier between graphene and a superconductor should exhibit oscillations[13] as a function of barrier strength, surprisingly peaking at finite values. These unexpected effects arise in large part from the hexagonal symmetry of graphene, which generates a relativisticlike band structure[5] near six points on the Fermi surface: the so-called Dirac points. The low-energy dispersion near these points is *linear*, and subsequently, the quasiparticles are governed by a two-dimensional massless Dirac-like equation.

Superconducting proximity effects in conventional heterostructures consisting of a normal metal and superconductor have been known for a very long time.[14] If the superconductor is coupled to a graphene sheet, where "Dirac quasiparticles" are confined to a two-dimensional plane, the leakage of superconductivity into graphene should exhibit novel behavior. Thus, studying superconducting proximity effects in graphene requires a careful and accurate determination of the pair correlations throughout the entire system. These are characterized by the pair potential $\Delta(\boldsymbol{r})$, and the pair amplitude, $F(\boldsymbol{r})$. A proper delineation of the associated proximity effects can only be achieved through a self-consistent calculation of $\Delta(\boldsymbol{r})$, ensuring that the system's lowest free-energy state is found. The resultant self-consistent state generally possesses nontrivial spatial inhomogeneity that can have important consequences for quasiparticle bound states, interface bound states,[15] and potential supercurrent flow. It is not surprising then that the frequently used step-function model for $\Delta(\boldsymbol{r})$, while satisfactory for length scales much longer than the superconducting coherence length, ξ_0, can lead to erroneous results for small graphene structures where quantum scale oscillations play a role. For example, superconductor widths that are on the same order as ξ_0 give rise to self-consistent pair potentials that can vary over a significant fraction of the total sample width. Moreover, self-consistency is crucial at finite temperatures, where the superconducting correlations can have substantial decay near the interfaces.

The usual superconducting proximity effect is governed by the mechanism of Andreev reflection. This is the process where at the interface, an electron with energy below the superconducting energy gap is retroreflected as a hole,

transmitting a Cooper pair into the superconductor. In graphene, the effectiveness of the Andreev process depends in part on the relative doping in the S and N regions. For electron doping the Fermi level is shifted upward, while for hole doping, it is shifted downward relative to the Dirac point. If the normal graphene layer is weakly doped, so that its Fermi level, μ_N, is in absolute value much smaller than that in the S region ($|\mu_N/\mu_S| \ll 1$), *specular* Andreev reflection becomes important. In this process, the electron and hole belong to different bands.[16] Thus, despite large Fermi wave-vector mismatch, superconducting correlations can penetrate into the normal graphene region. If, on the other hand, $\mu_N/\mu_S \gg 1$, both the conventional and specular Andreev reflection processes are suppressed and normal scattering drives the quasiparticle trajectories. The doping level clearly then has important consequences for any thermodynamic and transport properties involving superconducting graphene nanojunctions.

Besides doping effects, there are geometrical issues to contend with in finite S|N nanojunctions: The electronic structure of confined graphene can lead to a strong size dependence.[17] Depending on the widths of the normal graphene and superconducting regions, there are various energy scales that can be difficult to disentangle. If a S|N|S heterostructure has a thin middle channel of width d_N much smaller than ξ_0 (the superconducting coherence length), the relevant low-energy scale is the usual energy gap, Δ_0. This holds then for superconducting graphene,[18] which behaves, in this case and in this respect, the same way as conventional three-dimensional materials.[19,20] Short structures also result in critical currents that can deviate from the simple harmonic form.[21] For wide middle layers, with $d_N \gg \xi_0$, the Thouless energy, $E_T \equiv v_f/d_N$, (v_f is the Fermi velocity) emerges as an important energy scale.[22] The Thouless energy in clean systems gives rise to geometry-dependent quantum phenomena that arise from the cumulative phase coherent effect of propagation and reflections from the structure boundaries. This energy scale interacts then with the Δ_0 scale: For large normal graphene widths, E_T can be smaller than Δ_0, and the energy spectrum possesses a Thouless gap for quasiparticles with energies less than a characteristic energy of order E_T. When E_T is of the same order as Δ_0, identifying the origin of spectral anomalies can be difficult. For long S|N|S heterostructures, the resultant peaks in quasiparticle spectra would be [assuming a non-self-consistent step function form for $\Delta(\boldsymbol{r})$] located at energies proportional to integer multiples of E_T.[22] Self-consistency can modify this result, however, as the pair potential deviates substantially from a simple step function model. Moreover, when the doping amount changes, this picture becomes complicated by changes in quasiparticle bound states and density of states (DOS) due to the shifting of the Fermi level.

In this paper we use a fully self-consistent framework to calculate the energy spectrum and pair amplitude in S|N|S graphene heterostructures. In addition to the self-consistent pair amplitude, our accurate numerical diagonalization method allows us to investigate two important quantities that can be measured experimentally and further clarify proximity effects in graphene. The first is the local DOS, which can be measured directly with a scanning tunneling microscope. The vanishing of the DOS at the Fermi energy in undoped graphene results in varying subgap bound states and minigaps[23] associated with the interplay between E_T and Δ_0. To effectively characterize the local electronic properties, we examine the DOS, in both the S and the N regions. The energy spectra reveal conditions for fully gapped and gapless states in graphene S|N|S junctions. For a given doping level, the gap width and magnitude are shown to diminish as d_N increases. The greatest variations are found to occur when $E_T < \Delta_0$.

The second experimentally observable quantity of interest is the critical temperature, T_c. We study how T_c varies as a function of doping levels and of the geometrical parameters. Our self-consistent calculations find a nontrivial variation in T_c as a function of the relative doping levels, μ_N/μ_S. The sensitivity of T_c on the Fermi shifts depends strongly on the width of the outer S regions: Thin superconductors with $d_S < \xi_0$ reveal the most drastic changes in T_c for small increments in doping. We show that, for particular ranges of d_S, d_N, and temperature, a S|N|S nanostructure can act as a type of switch that transitions between a superconducting and resistive normal state as the ratio μ_N/μ_S is varied, something that might be done by using a modulated in-plane external electric field.[1,24]

Despite the importance of self-consistency, the only previous self-consistent works addressing proximity effects in S|N|S structures are Josephson junction studies based on an attractive Hubbard model with the superconductivity arising from both external contacts and doping[25] or external contacts alone.[26,27] We use here instead the usual graphene Hamiltonian in wave vector space. The two approaches each have advantages and disadvantages that may be said to make them complementary. Tight-binding methods of the Hubbard type are a more powerful way to study transport phenomena such as Josephson currents, as done in the above-cited papers, while our framework provides a more convenient method to study quasiparticle spectra with the needed resolution to characterize the different energy scales. By doing this, we are able to easily study large-scale systems as well as narrow channels and larger coherence lengths. Also, our framework provides a way to study quasiparticle spectra with the needed resolution to sort out the various energy scales involved. For these purposes the real-space tight-binding set of equations are perhaps more computationally demanding than their wave vector counterparts. Our method also permits a straightforward analytical development of a linearized set of equations that allow efficient investigation of the critical temperature. The calculation of T_c has not yet been attempted by tight-binding methods. Thus, there is hardly any overlap between our self-consistent results and previous ones. The methods we use, then, provide a suitable way to calculate the critical temperature and are applicable for a wide range of geometrical and coherence lengths. We implement our method by numerically solving the microscopic Dirac Bogoliubov–de Gennes (DBdG) equations self-consistently in the continuum regime. By this procedure we can accurately represent the important geometrical effects inherent to finite-sized junctions. The DBdG equations are ideal for inhomogeneous S|N|S heterostructures since they give directly the quasiparticle amplitudes and energies that characterize proximity effects. They are also appropriate for clean systems such as graphene which has high electron mobility. To investigate the potential of our S|N|S system as a superconducting graphene switch, we determine the critical

temperature self-consistently. This is accomplished by taking the full DBdG equations and linearizing them via standard perturbative techniques. We then arrive at an essentially analytical method that determines the critical temperature as a function of geometrical parameters and doping levels.

This paper is organized as follows. In Sec. II, we introduce the continuum DBdG equations and the self-consistent theoretical methods we use to calculate the pair amplitude and local DOS. We then present our linearization method for calculating T_c. Section III contains our results and is divided into four subsections. In Sec. III A we discuss the proximity effect associated with the leakage of pairing correlations into the normal region, as well as the pair amplitude decay in the S regions, sometimes called the inverse proximity effect. In Sec. III B, the relevant energy scales are revealed in the local DOS. The energy gap in the quasiparticle spectra and its relation to doping levels is presented in Sec. III C. We discuss thermal effects in Sec. III D, where the critical temperature for our S|N|S structures is shown as well as the switching mechanism. Finally, Sec. IV contains some concluding remarks.

II. METHOD

The geometry we study consists of a graphene sheet infinite in one direction (that of the y axis) and composed of two doped strips of superconducting material, each of width d_S, separated by a normal region of width d_N (see Fig. 1). We consider the pairing in the S regions to be conventional s-wave. The methods we use to self-consistently diagonalize the mean-field single-band Hamiltonian are extensions of those previously employed[28–31] to study proximity effects in ordinary three-dimensional materials, but important changes have to be made to take into account the reduced dimensionality and the peculiar band structure of graphene. These changes are the focus of the discussion below.

Our starting point in this case is the DBdG equations which govern the quasiparticle spectrum of graphene. In the absence of magnetic effects, the DBdG equations for the two valleys $K(+)$ and $K'(-)$ are[16]

$$\begin{pmatrix} \mathcal{H}^{\pm} - \mu\hat{I} & \Delta\hat{I} \\ \Delta^{*}\hat{I} & -(\mathcal{H}^{\pm} - \mu\hat{I}) \end{pmatrix} \begin{pmatrix} \Psi^{\pm}_{u,n} \\ \Psi^{\mp}_{v,n} \end{pmatrix} = \epsilon_n \begin{pmatrix} \Psi^{\pm}_{u,n} \\ \Psi^{\mp}_{v,n} \end{pmatrix}. \quad (1)$$

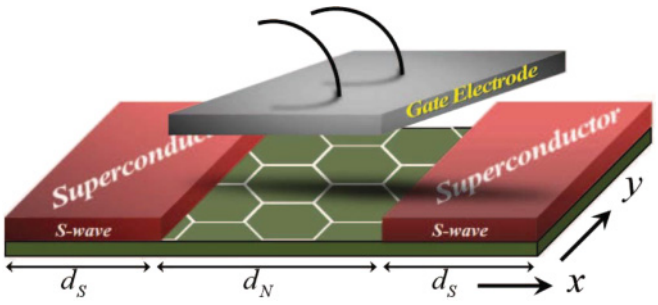

FIG. 1. (Color online) Schematic of the S|N|S graphene nanostructure studied. The sample is in the x-y plane. The widths of the superconducting and normal segments are d_S and d_N, respectively. The electrostatic potential in the normal region might be controlled via a gate voltage.

We consider low-energy excitations so that lattice effects are unimportant and the energy dispersion of the Dirac Hamiltonian, $\mathcal{H}^{\pm}$, is linear:[4,5,12] $\mathcal{H}^{\pm} = v_f(\sigma_x p_x \pm \sigma_y p_y)$. Here the σ_i are the 2×2 Pauli matrices acting in sublattice space, $\hat{I}$ is the identity matrix, and v_f is the (energy independent) Fermi velocity in graphene. The chemical potential μ vanishes in the undoped case but not in the presence of doping. Here we take $\mu(x)$ to be a piecewise constant: a fixed positive number μ_S in the S region and a variable value μ_N in the N regions. The electrostatic potential U_N (and consequently μ_N) in the N region may be controlled via an external gate voltage, as shown in Fig. 1. We consider the case of relatively large doping in the S regions, so that we can assume smooth interfaces.[16,26] We take these interfaces in the direction of constant x. We have defined $\Psi^{+}_{u,n} \equiv (u^n_{A,K}, u^n_{B,K})^T$, $\Psi^{-}_{u,n} \equiv (u^n_{A,K'}, u^n_{B,K'})^T$, $\Psi^{+}_{v,n} \equiv (v^n_{A,K}, v^n_{B,K})^T$, and $\Psi^{-}_{v,n} \equiv (v^n_{A,K'}, v^n_{B,K'})^T$. The A,B labels denote the two sublattices that arise from the honeycomb lattice structure.

The notation in the Hamiltonian implies that the Pauli matrices act on the pseudospin of the quasiparticles, mapping the usual spin into the projection of the wave function onto sublattice A or B. Since the valleys are degenerate (K and $-K'$ are equivalent), we need only solve for either $\mathcal{H}^{+}$ or $\mathcal{H}^{-}$. Assuming the first choice, we define the four component vector $\Psi_n \equiv (\Psi^{+}_{u,n}, \Psi^{-}_{v,n})$.

The pair potential Δ couples electrons in a given valley with the hole excitations in the other valley. In terms of the wave functions and energies obtained from Eq. (1), this coupling leads to the self-consistency condition,

$$\Delta(x) = \frac{g}{2}\sum_n \left[u^n_{A,K} v^{n*}_{A,K'} + u^n_{B,K} v^{n*}_{B,K'}\right] \tanh\left(\frac{\epsilon_n}{2T}\right), \quad (2)$$

where the superconducting coupling parameter, g, is a positive constant in the intrinsically superconducting regions and zero elsewhere. The sum is over all energy eigenstates within the Brillouin zone whose energy, referred to μ_S, is smaller than or equal to a characteristic energy cutoff, ω_c. (The overall spectrum is obtained over a range of energies several times larger.) It is to be interpreted as $\sum_n \to 1/(2\pi)\int dk_y \sum_q$, where k_y is the transverse momentum and q a longitudinal index. The singlet pairing only occurs from opposite valleys, to maintain time-reversal symmetry.[12,16]

The experimentally important local DOS, $N(x,\epsilon)$, is given by

$$N(x,\epsilon) = -\sum_{n,\alpha,\beta}\left[\left|u^n_{\alpha,\beta}\right|^2 f'(\epsilon-\epsilon_n) + \left|v^n_{\alpha,\beta}\right|^2 f'(\epsilon+\epsilon_n)\right], \quad (3)$$

where α equals A or B, β can be either K or K', and f' is the derivative of the Fermi function. One can integrate $N(x,\epsilon)$ over any suitable range of x to obtain the average DOS in a certain region.

We now take advantage of the translational invariance along y by writing $\Psi_n(x,y) \equiv e^{ik_y y}\Phi_n(x)$. Introducing the notation $\Phi^T_n(x) \equiv \big(s_n(x), t_n(x), w_n(x), z_n(x)\big)^T$ where the functions in the parenthesis correspond to valley and sublattice indices in the same order as for the previously defined Ψ_n, we can rewrite

the DBdG equation Eq. (1) as

$$\begin{pmatrix} -\mu & \pi_+^\dagger & \Delta & 0 \\ \pi_-^\dagger & -\mu & 0 & \Delta \\ \Delta^* & 0 & \mu & \pi_+ \\ 0 & \Delta^* & \pi_- & \mu \end{pmatrix} \begin{pmatrix} s_n \\ t_n \\ w_n \\ z_n \end{pmatrix} = \epsilon_n \begin{pmatrix} s_n \\ t_n \\ w_n \\ z_n \end{pmatrix}, \tag{4}$$

where we define $\pi_\pm \equiv i v_f(\partial_x \pm k_y)$ (we use $\hbar = 1$ and $k_B = 1$ throughout this paper).

Next we expand the quasiparticle wave functions via

$$\Phi_n(x) = \sum_{q=1}^{N} \boldsymbol{c}_{n,q} \phi_q(x), \tag{5}$$

where the $\boldsymbol{c}_{n,q} \equiv (s_{n,q}, t_{n,q}, w_{n,q}, z_{n,q})^T$ are the expansion coefficients and the $\phi_q(x)$ is a set of N basis functions, where N must be sufficiently large.[28,29] We take, consistent with the boundary conditions, $\phi_q(x) \equiv \sqrt{2/d}\sin(k_q x)$ in which $d = 2d_S + d_N$, and $k_q = q\pi/d$ is the quantized wave number. These basis functions are not eigenstates of the normal Hamiltonian. Therefore, there are $\pi^\pm$ off-diagonal terms. These introduce some computational challenges that result in a larger value of N being required than in the three-dimensional cases. Considering then each row of Eq. (4), we perform the following somewhat lengthy but elementary steps. First, we insert the expansion Eq. (5) into Eq. (4). Next, we multiply each term by $\phi_{q'}$ and integrate the variable x over the range $0 \leqslant x \leqslant d$, taking into account properly the stepwise x dependence of μ. Finally, we choose μ_S as our unit of energy (recall that we are dealing with a strongly doped system, so this quantity does not vanish) and divide through by μ_S.

Taking the same steps for the rest of the matrix, we end up with the following $4N \times 4N$ matrix equation:

$$\mathbf{M}\boldsymbol{a}_n = \widetilde{\epsilon}_n \boldsymbol{a}_n, \tag{6}$$

where

$$\mathbf{M} = \begin{pmatrix} \mathcal{A} & \mathcal{B} - i\widetilde{k}_y\mathbb{I} & \mathcal{D} & \mathbb{O} \\ \mathcal{B} + i\widetilde{k}_y\mathbb{I} & \mathcal{A} & \mathbb{O} & \mathcal{D} \\ \mathcal{D}^* & \mathbb{O} & -\mathcal{A} & -(\mathcal{B} - i\widetilde{k}_y\mathbb{I}) \\ \mathbb{O} & \mathcal{D}^* & -(\mathcal{B} + i\widetilde{k}_y\mathbb{I}) & -\mathcal{A} \end{pmatrix}, \tag{7}$$

and the vector, $\boldsymbol{a}_n$, contains the expansion coefficients,

$$\begin{aligned} \boldsymbol{a}_n \equiv (&s_{n,1}, \ldots, s_{n,N}, t_{n,1}, \ldots, t_{n,N}, \\ &w_{n,1}, \ldots, w_{n,N}, z_{n,1}, \ldots, z_{n,N})^T. \end{aligned} \tag{8}$$

Here $\mathbb{I}$ and $\mathbb{O}$ are unit and zero matrices of rank N, respectively. Consistent with our choice of energy units, we now define tilded dimensionless energies $\widetilde{\mu}_N \equiv \mu_N/\mu_S$ and $\widetilde{\epsilon}_n \equiv \epsilon_n/\mu_S$. We choose also to measure our wave vectors in units of k_{FS} defined by the relation $k_{FS} \equiv \mu_S/v_f$, thus, for example, $\widetilde{k}_y \equiv k_y/k_{FS}$ and then we have for the remaining elements in Eq. (7):

$$\begin{aligned} \mathcal{A}_{q,q'} = {} & \mathcal{K}_{q+q'}(d_S) - \mathcal{K}_{q-q'}(d_S) - \widetilde{\mu}_N[\mathcal{K}_{q-q'}(d_S + d_N) \\ & - \mathcal{K}_{q+q'}(d_S + d_N) - \mathcal{K}_{q-q'}(d_S) + \mathcal{K}_{q+q'}(d_S)] \\ & + \mathcal{K}_{q-q'}(d_S + d_N) - \mathcal{K}_{q+q'}(d_S + d_N), \quad q \neq q', \end{aligned} \tag{9}$$

$$\begin{aligned} \mathcal{A}_{q,q} = {} & \mathcal{K}_{2q}(d_S) - \frac{d_S}{d} - \widetilde{\mu}_N\left[\frac{d_N}{d} + \mathcal{K}_{2q}(d_S)\right. \\ & \left. - \mathcal{K}_{2q}(d_S + d_N)\right] - \frac{d_S}{d} - \mathcal{K}_{2q}(d_S + d_N), \end{aligned} \tag{10}$$

$$\mathcal{B}_{q,q'} = \frac{2iq'q}{k_{FS}d}\left(\frac{-1 + (-1)^{q+q'}}{q^2 - q'^2}\right), \quad q \neq q', \tag{11}$$

and $\mathcal{B}_{q,q} = 0$. Here $\mathcal{K}_n(x) \equiv \sin(n\pi x/d)/(n\pi)$. Finally,

$$\mathcal{D}_{q,q'} = \frac{2}{d}\frac{\Delta_0}{\mu_S}\int_0^d dx \sin(k_q x)(\Delta(x)/\Delta_0)\sin(k_{q'}x), \tag{12}$$

where Δ_0 is the order parameter in bulk S material at $T = 0$. The self-consistency relation Eq. (2) can now be written as

$$\begin{aligned} \Delta(x)/\Delta_0 = {} & 4\lambda\left(\frac{\xi_0}{d}\right)\int_0^{k_c} d\widetilde{k}_y \sum_n \sum_{q,q'} (s_{n,q} w^*_{n,q'} + t_{n,q} z^*_{n,q'}) \\ & \times \sin(k_q x)\sin(k_{q'}x)\tanh\left(\frac{\epsilon_n}{2T}\right), \end{aligned} \tag{13}$$

where[32] $\xi_0 = v_f/\Delta_0$, k_c is the $\widetilde{k}_y$ cutoff corresponding to those states specified below Eq. (2), and λ is the *dimensionless* coupling constant which we define as $\lambda \equiv g\mu_S/2\pi v_f^2$. Since the DOS for bulk S material in its normal state is $N_0(\epsilon) = 2\epsilon/(\pi v_f^2)$, we have $\lambda = gN_0(\mu_s)/4\pi$.

To perform our calculations, we must solve Eq. (6) together with the self-consistency condition Eq. (13). When $\widetilde{\omega}_c \equiv \omega_c/\mu_S$ satisfies $\widetilde{\omega}_c \leqslant 1$, we find for the bulk case

$$\lambda^{-1} = \operatorname{arcsinh}(\omega_c/\Delta_0), \tag{14}$$

while if $\widetilde{\omega}_c \geqslant 1$, then[32]

$$\lambda^{-1} = \sqrt{\widetilde{\Delta}_0^2 + \widetilde{\omega}_c^2} - \sqrt{\widetilde{\Delta}_0^2 + 1} + \operatorname{arcsinh}(1/\widetilde{\Delta}_0), \tag{15}$$

where $\widetilde{\Delta}_0 \equiv \Delta_0/\mu_S$. To achieve self-consistence, we start with an initial guess for $\Delta(x)$ and once all of the eigenfunctions and eigenenergies have been determined, we calculate a new $\Delta(x)$ from Eq. (13) and iterate this process until the relative difference between successive $\Delta(x)$ is less than 10^{-4}.

We also determine the critical temperature, T_c, semianalytically as a function of the geometrical and doping parameters. To find T_c, the self-consistency equation can be linearized[31] near the transition, leading to the form

$$\Delta_i = \sum_q J_{iq}\Delta_q, \tag{16}$$

where the Δ_i are expansion coefficients of the pair potential [Eqs. (2) and (13)] in our basis and the J_{iq} are the appropriate matrix elements with respect to the same basis, as obtained from the linearization procedure. These matrix elements can be written as $J_{iq} \equiv (J^u_{iq} + J^v_{iq})/2$, where

$$J^u_{iq} = \gamma\int d\widetilde{k}_y \sum_n^{N_D}\left[\tanh\left(\frac{\widetilde{\epsilon}^{u,0}_n}{2T}\right)\sum_m^N \frac{\mathcal{F}_{qnm}\mathcal{F}_{inm}}{\widetilde{\epsilon}^{u,0}_n - \widetilde{\epsilon}^{v,0}_m}\right], \tag{17}$$

$$J^v_{iq} = \gamma\int d\widetilde{k}_y \sum_n^{N_D}\left[\tanh\left(\frac{\widetilde{\epsilon}^{v,0}_n}{2T}\right)\sum_m^N \frac{\mathcal{F}_{qmn}\mathcal{F}_{imn}}{\widetilde{\epsilon}^{v,0}_n - \widetilde{\epsilon}^{u,0}_m}\right]. \tag{18}$$

Here $\gamma = \lambda/(2\pi^2 k_{FS} d)$, with λ the *dimensionless* superconducting coupling constant introduced above. The eigenenergies, $\epsilon_n^{u(v),0}$, are the unperturbed particle (hole) energies [found by setting $\Delta = 0$ in Eq. (4)], and N_D denotes that the sum is cut off at energies beyond the ω_c frequency. We also have

$$\mathcal{F}_{qnm} \equiv \pi\sqrt{2d}\sum_{p,r}^{N} \mathcal{K}_{qpr}(s_{nr} w^*_{mp} + t_{nr} z^*_{mp}), \tag{19}$$

where the correlation factor, $\mathcal{K}_{qpr}$, is written,

$$\mathcal{K}_{qpr} \equiv (2/d)^{3/2}\int_0^d dz\Theta(z)\sin(k_q z)\sin(k_p z)\sin(k_r z). \tag{20}$$

Here we define $\Theta(z)$ to be unity in the superconducting regions and vanish in the normal ones. The determination of T_c involves calculating the eigenvalues of matrix J_{iq} for each temperature value in the range of interest, and the highest temperature for which the largest eigenvalue of the matrix J_{iq} is unity[33,34] corresponds to T_c. This linearization route is much more efficient at calculating T_c than solving the full DBdG equations near T_c, which can often be very difficult due to the large number of iterations involved in the self-consistency process.

III. RESULTS AND DISCUSSION

In this section, we present our self-consistent results for the pair amplitude, local DOS, and critical temperature, for a broad range of widths and relative doping levels. We consider the S regions to be electron doped, corresponding to $\mu_S > 0$, while the normal graphene can be electron doped ($\mu_N > 0$), hole doped ($\mu_N < 0$), or undoped ($\mu_N = 0$). All lengths are scaled in units of the Fermi wave vector k_{FS}, and we define the relative dimensionless coordinate $X \equiv k_{FS}(x - d/2)$, so that $X = 0$ is at the center of the structure. When considering thermal effects, all quantities involving the temperature, T, are scaled by T_0, the transition temperature for the bulk superconducting material. Our input parameters are, besides the geometrical lengths, which are given in dimensionless form as $D_S \equiv k_{FS} d_S$ and $D_N \equiv k_{FS} d_N$, the value of $\widetilde{\mu}_N$ and that of the dimensionless coherence length $\Xi_0 \equiv k_{FS}\xi_0 = 100$. From the latter, and using a fixed value of $\widetilde{\omega}_c = 0.04$ (for $\omega_c < 1$, results are only weakly sensitive to ω_c) we obtain λ via Eq. (14).

A. Proximity effects: The pair amplitude

We first consider our results for the self-consistent normalized Cooper *pair amplitude* $F(x) \equiv (1/\lambda)\Delta(x)/\Delta_0$, which reveals the superconducting correlations throughout the entire S|N|S system. Some of our results for $F(X)$ as a function of dimensionless distance X are shown in Figs. 2 and 3. In Fig. 2, $F(X)$ is shown, in each panel, for a different value of D_N, all at the same $D_S = 150$. Several (all positive) values of the relative doping parameter $\widetilde{\mu}_N$, corresponding to electron doping, are shown in this figure: The undoped N case is also shown for comparison. We see that the proximity effect depends strongly on the relative doping $\widetilde{\mu}_N$ via the mismatch it reflects (when this quantity is unity, there is no mismatch). Moderate doping in the N region exemplifies the proximity effect where appreciable pairing correlations exist in the

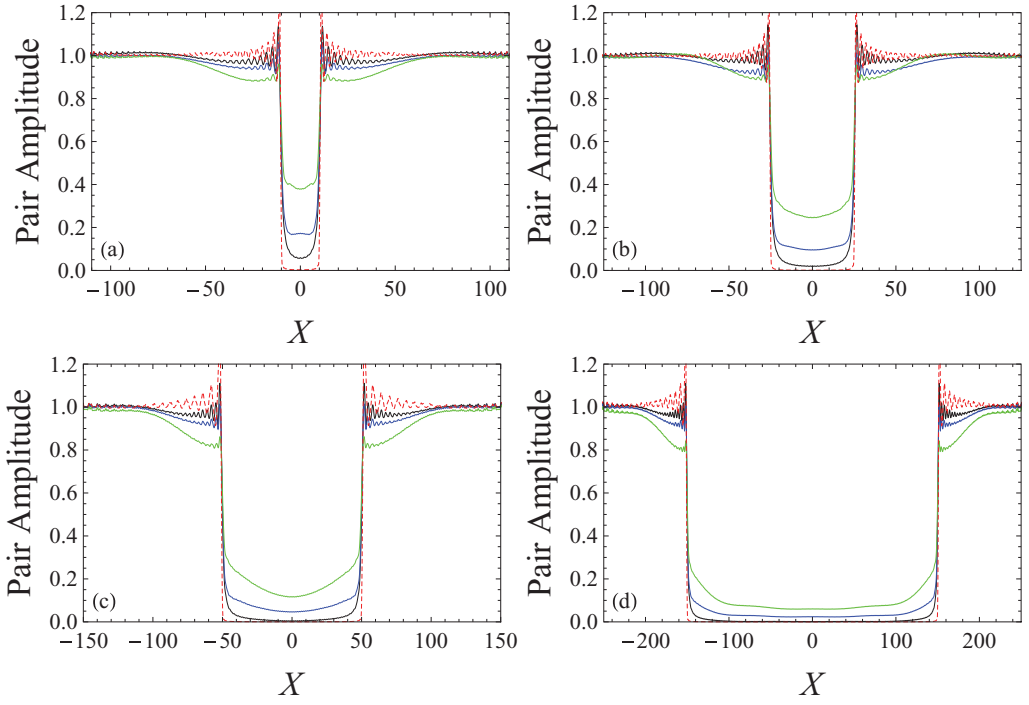

FIG. 2. (Color online) Normalized pair amplitude vs X (see text) at $T = 0$ for an S|N|S heterostructure. The S portions have a dimensionless width (see text) of $D_S = 150$ each. For clarity, the outermost parts of the sample are not shown. Each panel corresponds to a different normalized normal graphene width of (a) $D_N = 20$, (b) $D_N = 50$, (c) $D_N = 100$, and (d) $D_N = 300$. For each case, four curves representing different doping levels are shown. From top to bottom in the central N region (green, blue, black, red), these curves correspond to $\widetilde{\mu}_N = 0.5, 0.2, 0$, and 10.

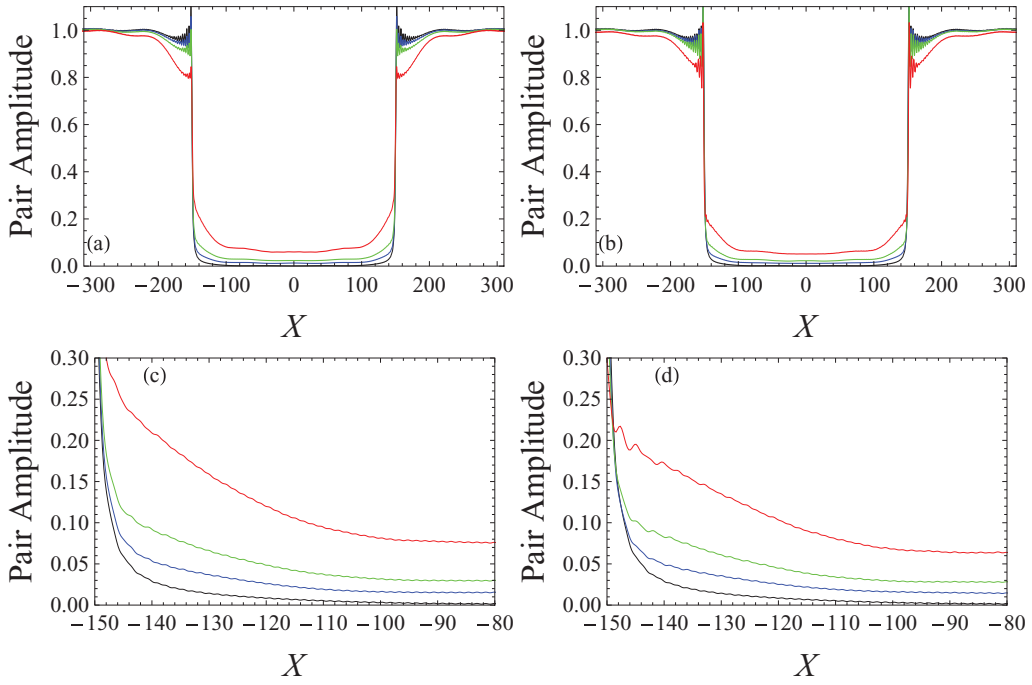

FIG. 3. (Color online) Normalized pair amplitude versus X, as in Fig. 2. The dimensionless geometrical quantities D_N and D_S are now $D_N = 300$ and $D_S = 300$, so that the S|N boundaries are at $|X| = 150$. The top set of panels depicts most of the S|N|S structure and the bottom set of panels shows a magnified part of the N region near the interface for the panel above it. Panels (a) and (c) are for electron-doped N with curves shown, from top to bottom at $X = 0$, for $\widetilde{\mu}_N = 0.5$, 0.2, and 0.1 (red, green, and blue), while panels (b) and (d) are for hole-doped N with $\widetilde{\mu}_N = -0.1$, -0.2, and -0.5 with a similar scheme. In both cases results for $\widetilde{\mu}_N = 0$, (black) lowest curve at $X = 0$, are shown for reference.

normal graphene, even when $D_N > \Xi_0$ (right bottom panel), as one can see, for example, in the $\widetilde{\mu}_N = 0.5$ [(green) highest curves at $X = 0$] results shown. Correspondingly, depletion of $F(X)$ in the S regions extends in this case to distances longer than the correlation length (strong inverse proximity effect). On the other hand, when the mismatch in the Fermi shifts is extreme as in the $\widetilde{\mu}_N = 0$ (black solid curve, third from top at $X = 0$) and $\widetilde{\mu}_N = 10$ (red dashed curves) cases shown, we see that the proximity effect is much weaker. The blue solid curves, second highest at $X = 0$, corresponding to $\widetilde{\mu}_N = 0.2$, show intermediate behavior. Further examination of the results in this figure for large mismatch ($\widetilde{\mu}_N = 0$) reveals that the presence of evanescent modes in this case can allow more readily for the penetration of correlations in the normal graphene than large mismatch in the opposite direction: Comparing the $\widetilde{\mu}_N = 0$ to the $\widetilde{\mu}_N = 10$ results, the self-consistent state in the later case shows less superconducting correlations in the normal graphene than in the former case and a correspondingly smaller depletion in the S layers. We also examined the case of small mismatch ($\mu_N/\Delta_0 = 0.5$ equivalent to $\widetilde{\mu}_N = 0.005$), where specular Andreev reflection can arise, and found no discernible differences in the pair amplitude compared with the $\widetilde{\mu}_N = 0$ case above (not shown). The sequence of panels, moreover, illustrates that increasing the N graphene widths always results (at the same value of $\widetilde{\mu}_N$) in greater superconductivity depletion in the S regions near the interfaces due to leakage into the N layer. The smaller the Fermi level mismatch, the greater this effect. For more confining N regions (smaller D_N), the pair correlations decay in the normal layer over a smaller width and thus the two superconductor portions of the sample are more strongly coupled. Some of the results in Fig. 2 bear qualitative resemblances to Fig. 3 of Ref. 25, where a tight-binding model was used. However, we find that the proximity effects and associated superconductor coupling appear more pronounced in the regime considered here. In particular even for $\widetilde{\mu}_N = 0$, the smaller N widths allow significant Cooper pair penetration, possibly related to the nonvanishing supercurrent flow reported in short Josephson junctions at the Dirac point.[18]

To better illustrate the proximity effect, the slow decay of the amplitude $F(X)$ in the normal graphene region, we display in Fig. 3, results for this normalized quantity obtained for a much larger system with $D_N, D_S > \xi_0$. We show there also results for a broader range of doping levels in N. The top set of panels shows a global view of the correlations in the S|N|S structure, similar to that shown in Fig. 2, while in the bottom set of panels are closeups of the normal graphene region near the interface. The electron-doped (left panels) cases are nearly identical to the hole-doped (right panels) ones, except at smaller mismatch. The bottom panels allow for a more detailed examination of the behavior near the interface. We note that, if the mismatch is not large, penetration of the Cooper pairs over a distance clearly much larger than the correlation length occurs and that depletion in the S regions occurs also in the same scale. On the other hand, one can see in both this and the previous figure that the transition between the depleted S region and the weakly proximity-influenced N region is very abrupt: There are, in effect, two length scales, one related

to the depletion and penetration, which can be rather longer than ξ_0, and another, very short scale, over which the small values of $F(X)$ in N transition sharply to the depleted, but much larger, values in S. This is in contrast to what occurs in the standard proximity effect in ordinary three-dimensional bilayer materials, which is characterized by a single length scale.[35]

B. Local density of states

Before discussing the local DOS for S|N|S structures, it is illuminating to first investigate the DOS and characteristic energies for pure graphene nanolayers, which we do by setting $D_s = 0$. In the absence of other materials, and hence also of proximity effects, the DOS in this case is essentially independent of position, and thus it is appropriate to spatially average Eq. (3) over the entire sample, which (after using the normalization condition for the quasiparticle amplitudes) yields a simplified normalized DOS,

$$\frac{N(\epsilon)}{N_0(\mu_S)} = \frac{v_f}{2Td}\sum_n \int_0^{k_c} d\widetilde{k}_y \left[\cosh^{-2}\left(\frac{\epsilon-\epsilon_n}{2T}\right) + \cosh^{-2}\left(\frac{\epsilon+\epsilon_n}{2T}\right)\right], \tag{21}$$

where T is the temperature and $N_0(\epsilon)$ is introduced below Eq. (13). In this case, with only normal material present, it must be understood that $N_0(\mu_s)$ is just an arbitrary, but convenient, normalization. Note that after setting $D_S = 0$ and hence $\Delta \equiv 0$, no iteration for self-consistency is needed and only the eigenvalue spectra needs to be determined when performing the diagonalization of the matrix in Eq. (4). To achieve the required energy resolution for the results to follow, integrals over k_y are numerically evaluated by transforming them into a sum over 5000 transverse modes. Also, in order to better discern the relevant DOS features, we consider the low-temperature limit (see below). For finite-width graphene sheets, the coherent superposition of standing waves determines the Thouless energy scale,[22]

$$E_T = \frac{v_f}{d_N}. \tag{22}$$

The Thouless energy scale reveals itself in the form of peaks in the quasiparticle spectra that, in this simple geometry repeat at odd integer multiples of $E_c = \pi E_T$. We have then $E_c/\mu_S = \pi/D_N$. The μ_S and k_{FS} act here as convenient arbitrary normalizations. These peaks are superimposed on the straight lines that would represent the DOS in the $D_N \to \infty$ limit. If one normalizes, as we do, the energies in terms of μ_S, and the DOS as explained above, then the slope of these straight lines would be ± 1. Our results are shown in Fig. 4. The top panels [(a) and (c)] show the DOS [calculated from and normalized as in Eq. (21)] over a broad energy range. Panel (a) is for undoped graphene ($\widetilde{\mu}_N = 0$) and panel (c) corresponds to a relative doping of $\widetilde{\mu}_N = 0.2$. For these two cases, there are four curves shown that correspond to four different graphene widths (see caption). The Thouless peaks are at their predicted positions. Their magnitude tends to decrease as the width increases, with the results for largest width, $D_N = 600$, approaching the signature linear dispersion for bulk graphene. With the introduction of doping [panel (c)] the results are shifted, in normalized energy units,

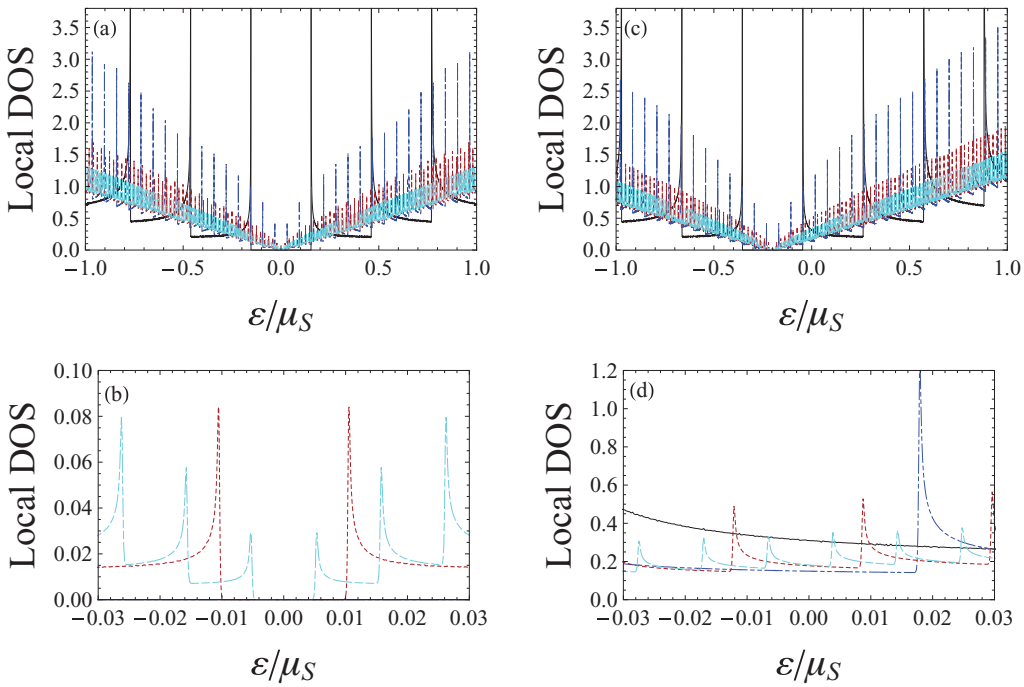

FIG. 4. (Color online) Local DOS for a normal, finite width, graphene layer that has (a) zero doping ($\widetilde{\mu}_N = 0$), and (c) moderate doping ($\widetilde{\mu}_N = 0.2$). The normalizations of DOS and energies are chosen (see text) so that for an infinite width layer the plots would be straight lines of slope ± 1. Four different widths are illustrated, in order of decreasing height of the main peaks: $D_N = 20$ (black), $D_N = 100$ (blue), $D_N = 300$ (red), and $D_N = 600$ (cyan). Each bottom panel is a magnification of the results above it, over a narrower energy range. The main peaks are related to the Thouless scale; see Eq. (22) and discussion below it.

by $-\widetilde{\mu}_N$ from the Dirac point, resulting in the shifting of the gap away from zero energy for all widths shown. To more clearly discern the Thouless peaks, the bottom panels, which correspond to the same parameter values as the top ones, illustrate the DOS over a smaller energy range. In Figs. 4(b) and 4(d), the Thouless peaks in the DOS are clearly seen to occur at energies that coincide with the expression discussed below Eq. (22): For $D_N = 300$, the first peaks arise at energies corresponding to $|E_c/\mu_S| = \pi/300 \approx 0.01$, while for $D_N = 600$, we have, $|E_c/\mu_S| = \pi/600 \approx 0.005$. In Fig. 4(b), the curves representing the smaller widths, and correspondingly larger E_T, are absent since [as panel (a) shows] they emerge beyond the given energy window. These results illustrate also the precision and reliability of our methods.

We now return to the S|N|S system and investigate the roles that both the Thouless and the superconducting energy scales play by considering the local DOS of a S|N|S nanostructure in both the S and the N regions. After inserting the quasiparticle expansions found in Eq. (5), the general expression for the DOS in Eq. (3) can be rewritten as

$$\frac{N(x,\epsilon)}{N_0(\mu_s)} = \frac{\mu_S}{Tk_{FS}d}\int_0^{k_c} d\widetilde{k}_y \Bigg[\Bigg(\Bigg|\sum_{n,q} s_{n,q}\sin(k_q x)\Bigg|^2 + \Bigg|\sum_{n,q} t_{n,q}\sin(k_q x)\Bigg|^2\Bigg)\cosh^{-2}\left(\frac{\epsilon-\epsilon_n}{2T}\right) + \left(\Bigg|\sum_{n,q} w_{n,q}\sin(k_q x)\Bigg|^2 + \Bigg|\sum_{n,q} z_{n,q}\sin(k_q x)\Bigg|^2\right) \times \cosh^{-2}\left(\frac{\epsilon+\epsilon_n}{2T}\right)\Bigg]. \quad (23)$$

In calculating the DOS for the S|N|S cases, we take the eigenvectors and eigenenergies, self-consistently calculated as explained above, and insert them into Eq. (23). When $\widetilde{\omega}_c < 1$, the case considered here, the relationship between the bulk transition temperature T_0 and Δ_0 is found using Eq. (14), together with[36]

$$\lambda^{-1} = \int_0^{\omega_c} \frac{d\xi}{\xi}\tanh[\xi/(2T_0)], \quad (24)$$

which results in the weak coupling limit in the BCS relation[32] $\Delta_0 = (\pi/\gamma_E)T_0$, with γ_E being the Euler constant. We take the low-temperature limit $T/T_0 \approx 0.016$. This is the same temperature as in the previous plots. The energy-resolved DOS is then determined at two locations: one at the middle of one of the superconducting regions and the other at the center of the sample (normal region). In these plots, we normalize the energy (measured, as usual, from the chemical potential) by Δ_0, and the plotted DOS (as before) by $N_0(\mu_S)$. Thus, if our plots were performed for an infinite normal sample, they would, of course, still be straight lines but the slope would now be $\pm\Delta_0/\mu_S$, which is the same as $1/\Xi_0$ via the relations mentioned in Sec. II.

There are now two energy scales to consider. One is, as ordinarily in all superconductors, the bulk gap Δ_0. In addition, because our system is two dimensional, has a linear, massless dispersion relation and is finite in the x direction, the DOS is also, as we have seen, drastically affected by the Thouless energy.[37] The quasiparticles in the previously discussed graphene nanostrip were confined solely by the two outer boundaries. Now due to the intrinsically superconducting regions, there is also possible partial confinement by the self-consistent pair potential $\Delta(x)$, which, due to Andreev scattering events (normal or specular), leads to a modification of the relevant energy scales associated with the peaks in the quasiparticle spectra. Thus, the two scales interact. For large N graphene widths ($d_N \gg \xi_0$), the normalized energy spectrum has the gap set primarily (not exclusively) by the Thouless characteristic energy, and a peak structure[22] at multiples of E_T. In the S|N|S geometry the relevant scale is now[38] $E_c = (\pi/2)E_T$. It follows then that $E_c/\Delta_0 = (\pi\,\Xi_0)/(2D_N)$. The interplay between this ratio and that of Δ_0 to μ_S can for a given energy range result in many additional resonance peaks. In the non-self-consistent treatment, and for energies larger than Δ_0, these peaks occur at integer multiples of E_T,[22] and the energy gap is governed by E_T (for $d_N \gg \xi_0$). The energy spectrum is more complicated in the subgap regime ($\epsilon < \Delta_0$), where additional peaks can arise depending on the relative energy scales: for energies less than Δ_0, Andreev scattering at the S|N interfaces that is specular ($\mu_N < \Delta_0$) or retroreflective ($\mu_N > \Delta_0$) can strongly affect the local DOS in the N region[40] (for μ_N nonzero). As is seen below, however, self-consistently accounting for proximity effects in our finite-sized system will in some cases modify this picture. Hence, as a consequence of the existence of the Thouless scale, the behavior of the local DOS in a S|N|S heterostructure is strongly dependent on the size of each region. If, however, the normal graphene channel is much narrower than ξ_0, the lowest energy scale is Δ_0.

To illustrate these issues, results for $D_S = 150 = 1.5\Xi_0$ and various values of D_N are exhibited in Fig. 5. The results in this figure correspond to very low doping in the N region, and include cases where $d_N < \xi_0$ and cases where it is larger, thus demonstrating the relative relevance of both the Δ_0 and E_T energy scales in different situations. Thus, consider first the local DOS in the N region that is undoped ($\widetilde{\mu}_N = 0$) and shown in the middle panels (c) and (d). In panel (d) we have $d_N = 3\xi_0$ (red solid curve) and $d_N = 6\xi_0$ (green dashed curve) so that the influence of the S portions of the sample is, while as we have seen not negligible, weak. One clearly sees that the results can still be described by a straight line of slope $1/\Xi_0 = 0.01$ on which there are superimposed peaks and oscillations related to both the Δ_0 and the E_T scales. For the parameter values in this panel we have (see discussion above) that when $\epsilon/E_c = 1$ then the normalized energy ϵ/Δ_0 is about $1/2$ for $d_N = 3\xi_0$ and half that for the other case shown. One sees indeed this behavior in this panel (d). On the other hand, in panel (c), where results for smaller values of D_N/Ξ_0 are shown, the influence of the Thouless scale is very weak for $d_N = \xi_0$ (blue dashed curve) when the two energy scales roughly coincide and nearly nonexistent when $d_N < \xi_0$ (black solid curve). Panels (e) and (f) display the local DOS in the N region for a nonzero but small μ_N ($\mu_N < \Delta_0$), corresponding to $\mu_N/\Delta_0 = 0.5$, and with all other system parameters the same as used for (c) and (d), respectively. In this regime, specular Andreev reflection arises and has been found to also play a major role in the transport characteristics of graphene based junctions.[16] This accounts

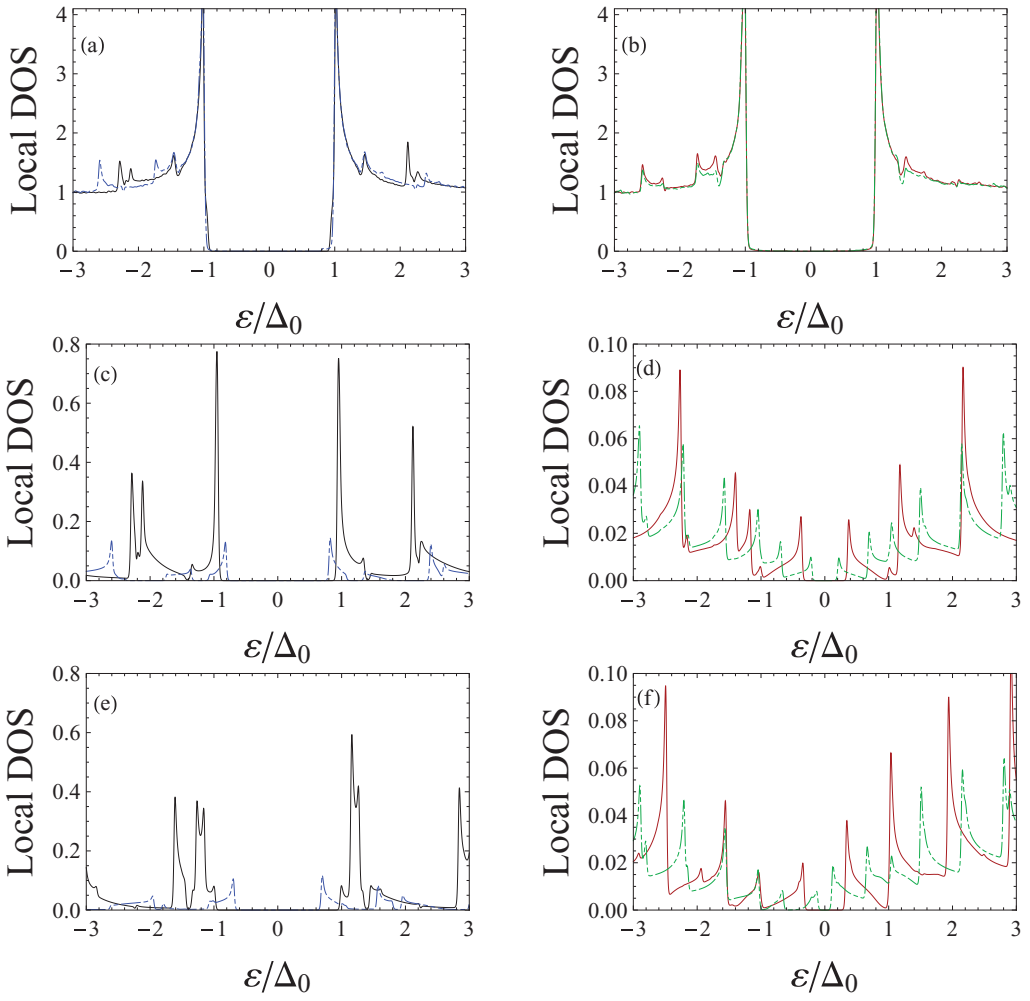

FIG. 5. (Color online) Local DOS (normalized as explained in the text) for S|N|S systems with both vanishing and very low doping in the N layers. Panels (a)–(d) correspond to $\widetilde{\mu}_N = 0$, while panels (e) and (f) correspond to $\widetilde{\mu}_N = 0.005$ (or equivalently $\mu_N/\Delta_0 = 0.5$). Results are shown for the S region [panels (a) and (b)] and in the N region [(c)–(f)]. In (a), (c), and (e) we have $D_N = \Xi_0/5$ (solid black curves) and $D_N = \Xi_0$ (blue dashed curves), while in (b), (d), and (f), the N layers are larger: $D_N = 3\Xi_0$ (solid red curves) and $D_N = 6\Xi_0$ (dashed green curves).

for the striking difference between the results in these panels and those in panels (c) and (d).

The results in Fig. 5 for the local DOS in the S region are very different. These are shown in panels (a) and (b) for the same values of D_N and the same plotting conventions as for panels (c) and (d), respectively. We show only the cases corresponding to an undoped N region ($\widetilde{\mu}_N = 0$), as the differences with the undoped and the slightly doped case ($\widetilde{\mu}_N = 0.005$) are now insignificant. We now see a very clear energy gap close to the bulk value. The influence of the Thouless energy is reduced now to some weak additional peaks at higher energy. We can see that at the energy scales shown the effect of the bulk normal state linear DOS is not visible, although of course this is an artifact arising from the energy range plotted and the increasing behavior reappears eventually at larger values of $\epsilon \gg \Delta_0$. Even though $\widetilde{\mu}_N = 0$, particle-hole symmetry breaks down in the N region.

The local DOS can be strongly or weakly dependent on the doping level, depending on the location within the structure. To show this we display in Fig. 6 results for the DOS at $\widetilde{\mu}_N = 0.2$. In this case, the DOS for bulk ($D_N \to \infty$) normal graphene (zero Thouless energy and zero pair potential) is still (see Fig. 4) a straight line but with the origin shifted. For our parameter values, and indeed for any reasonable parameter values in our context, this origin is shifted out of the horizontal scale in the energy ranges of order Δ_0 shown in this figure. The four panels in the figure are arranged exactly as the top four in Fig. 5 and correspond [both the panel arrangement and the (color or) structure of the curves] to exactly the same cases. One can see that when the doping amount changes, this DOS becomes more complicated because of changes in the quasiparticle bound states shifting with the Fermi level. Thus, the results for large D_N in the N region [panel (d)] show now only a faint trace of any gap, either superconducting or Thouless: The DOS is nearly linear at small energies, possessing a V shape at the Dirac point. This subgap structure may be related to the traditional Andreev bound states[39] that arise also in conventional, three-dimensional materials. They were recently studied (for $\mu_N \gg \Delta_0$) in the context of non-self-consistent graphene-based billiards.[40] The

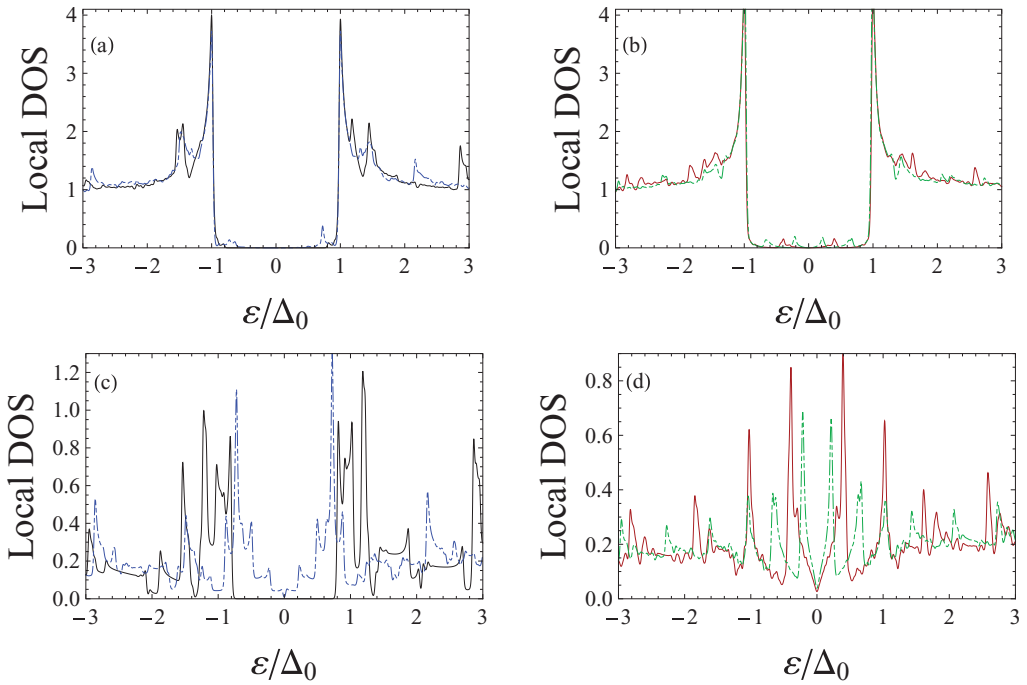

FIG. 6. (Color online) Local DOS (plotted and normalized as in Fig. 5) for an S|N|S system with moderately doped S layers ($\widetilde{\mu}_N = 0.2$). The panel arrangement, curve (color and) structure, and all other parameters are the same as that in Fig. 5. See text for discussion and comparison

suppression of the DOS in the N region may also be linked to billiard systems with integrable classical dynamics.[41] In panel (c), when the d_N is comparable to the correlation length, the "V" behavior still persists (dashed blue curve), but it is completely gone, and replaced by a gap, when the thickness is below ξ_0 (solid black curve). The panels (a) and (b), corresponding to the S region, are less strikingly different from the corresponding ones in Fig. 5. This relatively weak doping dependence in the local DOS in S agrees qualitatively with tight-binding results for an S|N junction;[25] however, in our structure we find an intriguing additional structure in the gap region.

C. Energy gap

In view of the strong effect, as evidenced in the comparison of Figs. 5 and 6, of $\widetilde{\mu}_N$ on the gap structure in the DOS it is interesting to further examine in a more direct way the induced gap in the quasiparticle spectrum. This we do by extracting from our numerical results the eigenvalue from the self-consistent spectra obtained from Eq. (6) for which ϵ_n as measured from the chemical potential is minimum. We call this quantity the excitation gap and denote it by $E_{\rm gap}$, which is generally determined by longitudinally directed (along x) trajectories corresponding to small k_y. The results are shown in Fig. 7, where we show the evolution of $E_{\rm gap}$ normalized by Δ_0 (so that the quantity plotted is non-negative and less than unity) as a function of $\widetilde{\mu}_N$. Results for four different values of D_N are shown, encompassing values both above and below Ξ_0: $D_N = 20 = 0.2\Xi_0$ (circles), $D_N = 50$, (squares), $D_N = 100$ (diamonds), and $D_N = 300$ (triangles). In all cases $D_S = 150$. The range of $\widetilde{\mu}_N$ and values of D_N that result in a gap are, of course, consistent with the DOS results above. The results shown illustrate that structures including narrower normal graphene layers possess energy gaps that are much more robust to changes in N layer doping. The contraction of the gap with increasing D_N is qualitatively similar to what is observed in conventional three-dimensional systems,[42] but, as mentioned above, the structure of the gap amplitude and of the DOS is very different.

D. Critical temperature and switching effects

Up to this point, we have considered the low-temperature limit. It is of interest both experimentally and theoretically to now turn our attention to the calculation of the critical temperature T_c of the S|N|S structures and its dependence on doping levels and geometrical parameters. This quantity

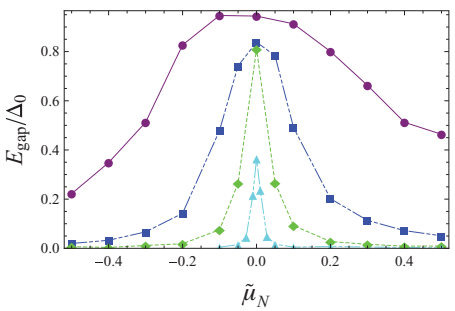

FIG. 7. (Color online) The excitation gap, $E_{\rm gap}$ as defined in the text, as a function of the relative doping parameter, $\widetilde{\mu}_N$. Four different normal graphene widths are considered: $D_N = 20$, 50, 100, and 300 (red circles, blue squares, green diamonds, and cyan triangles respectively). Lines are straight segments joining points.

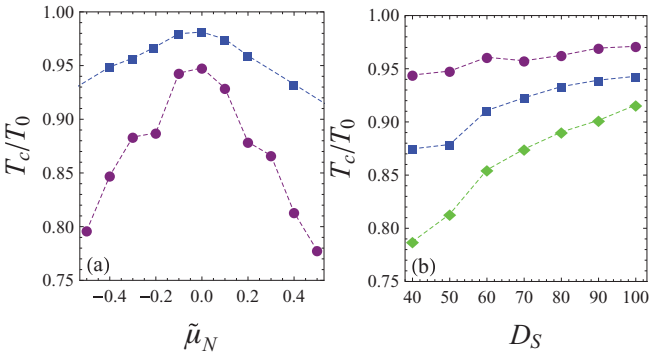

FIG. 8. (Color online) The critical temperature T_c (normalized by T_0) for a S|N|S system as a function of (a) $\tilde{\mu}_N$, and (b) the S width, D_S. In (a) the doping dependence is shown for two values of $D_S = 50$ (red circles) and 100 (blue squares). In (b), results are shown as a function of D_S for three doping levels: $\tilde{\mu}_N = 0$ (red circles), 0.2 (blue squares), and 0.4 (green diamonds). The doping level in these cases has a dramatic effect on T_c for small D_S, but is less detrimental for larger D_S, where the curves tend to coalesce in the limit of bulk S widths. In both (a) and (b), the normal graphene layer has $D_N = 100$.

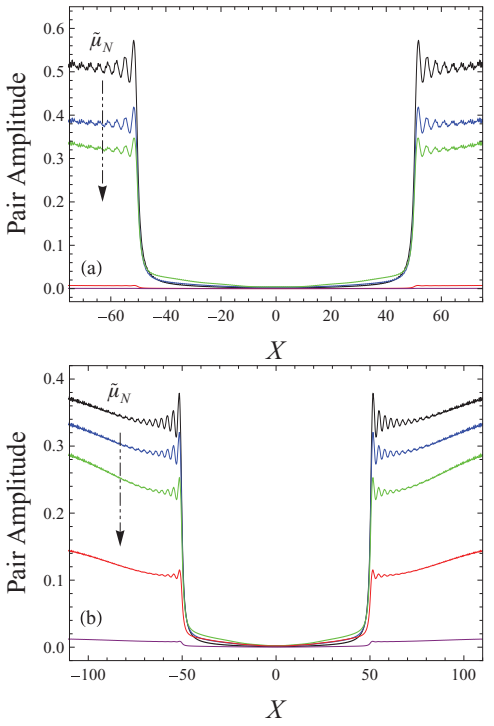

FIG. 9. (Color online) The normalized pair amplitude as a function of position. In (a), the temperature is set at $T = 0.87T_0$, and the normal and superconductor widths are $D_N = 100$ and $D_S = 50$, respectively. In (b), we have $T = 0.92T_0$, while $D_N = 100$ and $D_S = 100$. In both cases, the doping parameter, $\tilde{\mu}_N$, is varied from 0 to 0.4 in increments of 0.1. The arrow depicts the direction of increasing $\tilde{\mu}_N$, which eventually leads to the vanishing of the pairing correlations.

is calculated using the efficient eigenvalue method described by Eq. (16) and the discussion below it. Results are presented in terms of the ratio T_c/T_0 and displayed in Fig. 8. In the left panel, results are given as a function of relative doping level $\tilde{\mu}_N$ for two values of D_S: $D_S = \Xi_0 = 100$ (blue squares) and $D_S = \Xi_0/2$ (red circles). We keep $D_N = \Xi_0$ constant in this figure. We see than increasing $|\tilde{\mu}_N|$ to moderate values, that is, decreasing the Fermi level mismatch, leads to [Fig. 8(a)] a reduction in T_c via the corresponding increase in the interlayer coupling. This effect is more pronounced for thin S layers, where T_c can vary with $\tilde{\mu}_N$ in a nontrivial fashion. It is remarkable, however, that T_c remains rather high even when D_S is smaller than the correlation length. This is in stark contrast to ordinary three-dimensional S|N|S systems, where[42] T_c drops much more rapidly for small thicknesses satisfying $d_S \lesssim \xi_0$. There is also a clear asymmetry in the critical temperature as a function of doping, where for a given magnitude $|\tilde{\mu}_N|$, electron doping more strongly reduces T_c. In the right panel [Fig. 8(b)] we illustrate that varying the width of the superconductors has a considerably greater impact on T_c for moderate values of $\tilde{\mu}_N$ than when the mismatch is large. In the latter case the D_S dependence remains weak as long as D_S is still comparable to Ξ_0, however [and consistent with panel (a)] the superconducting regions that have widths a fraction of the coherence length reveal the richest behavior. Continuing to reduce D_S beyond some critical value, of course, results in the graphene system eventually becoming nonsuperconducting, as Cooper pair formation is inhibited.

Results such as those shown in Fig. 8(a) imply that at a fixed temperature, variations in the doping parameter, $\tilde{\mu}_N$, can lead to a S|N|S system transitioning from a superconducting state to normal one and vice versa. Since graphene doping can be effectively tuned via application of an external electric field,[1,24] this may offer possibilities as a carbon-based S|N|S switch for supercurrent flow. This question is, therefore, worthy of further discussion. We thus expand on this point by showing in Fig. 9 the normalized pair amplitude $F(X)$ plotted as a function of X for several positive values of $\tilde{\mu}_N$. Each panel is at a different fixed temperature and the geometrical parameters, $D_S = \Xi_0/2$ and $D_S = \Xi_0$ are chosen to correlate respectively with the (red) circled and (blue) squared data of Fig. 8(a). The two representative temperatures that we investigate are $T = 0.87T_0$ [panel (a)] and $T = 0.92T_0$ [panel (b)]. The graphene region that is intrinsically nonsuperconducting has a width in both cases corresponding to $D_N = \Xi_0$. One can see in Fig. 8(a) that for the smaller $D_S = \Xi_0/2$, the temperature $T = 0.87T_0$ corresponds to T_c near $\tilde{\mu}_N \approx 0.35$, and for $D_S = \Xi_0$, the temperature $T = 0.92T_0$ results in T_c near $\tilde{\mu}_N \approx 0.4$. The regions for which positive $\tilde{\mu}_N$ is smaller being superconducting (the corresponding negative $\tilde{\mu}_N$ differ slightly due to the electron-hole doping asymmetry). This is more clearly seen in Fig. 9, where as $\tilde{\mu}_N$ is increased, the pair amplitude is seen to decrease before plummeting abruptly to zero as $\tilde{\mu}_N$ reaches its critical value: near $\tilde{\mu}_N \to 0.35$ in panel (a) or near $\tilde{\mu}_N \to 0.4$ for panel (b). Thus, if this transition can be manipulated via electric fields, abrupt switching will result.

IV. CONCLUSIONS

We have studied in this paper the proximity effects that occur in clean, doped, and undoped, graphene-based S|N|S heterostructures. We have created and implemented a fully

self-consistent procedure to calculate the electron and hole wave functions and energy spectrum of the system, from which we have extracted the pair amplitude and the local DOS. We also developed a semianalytical and computationally efficient linearized method that can calculate the transition temperature, T_c, of the system.

We have found that the behavior of the pair amplitude near the interfaces (the directly observed proximity effect) depends strongly on the relative doping levels of the S and the N portions, and that the pair amplitude is described by two different length scales. One length scale is related to penetration of the superconducting correlations and is long ranged (relative to ξ_0) and the other scale is short ranged and correlates to Cooper pair leakage from the S regions near the interfaces. We illustrated that if the normal graphene layer is weakly doped, specular Andreev reflection can lead to superconducting correlations penetrating into the normal graphene region. The local DOS exhibits a number of striking features, arising from the interplay between the superconducting and the Thouless energy scales. This interplay depends, of course, on geometry, where the two energy scales overlap when the graphene layer widths are on the same order as ξ_0. For our larger structures (with widths exceeding ξ_0), undoped normal regions revealed resonant peaks and energy gaps at characteristic energies proportional to the Thouless energy scale E_T. By moderately doping the N region, there was an emergence of Andreev bound states in the N regions and a destruction of the energy gap. For N widths smaller than ξ_0, the S|N|S structures revealed energy gaps that are linked mainly to the Δ_0 scale, and are more robust to doping.

We also developed a general microscopic method for calculating T_c for S|N|S nanostructures, by linearizing the DBdG equations and the self-consistency condition. We found that for small S layer widths, decreasing the Fermi level mismatch leads to a nontrivial reduction in T_c. The critical temperature also exhibited a clear asymmetry as a function of doping, and typically electron doping had a greater impact on reducing T_c. Thus, if doping is to be modified by an electric field,[1,24] the polarity[43] of the field can have an important effect on the critical temperature. The study of T_c revealed reentrant behavior as a function of doping. These behaviors may lead to switching phenomena as a function of applied electric field, and thus, depending on the bias, superconductivity can be turned on or off. The effectiveness of graphene as a low-temperature-field effect device therefore depends in large part by the proximity effects, which can only be accounted for within a self-consistent framework. This work represents the first step, a proof of principle, as to the use of our self-consistent methods in graphene. Other issues, such as those related to ferromagnetically doped graphene in contact with a superconductor region,[44] can also be examined using the same techniques. We expect that many aspects of the ever-intriguing behavior of graphene-based heterostructures will be illuminated via application of these methods.

ACKNOWLEDGMENTS

This work is supported in part by ONR and by grants of HPC resources from DOD (HPCMP) and from the Minnesota Supercomputer Institute. M.A. wishes to thank J. Linder for conversations.

*klaus.halterman@navy.mil

†otvalls@umn.edu; also at Minnesota Supercomputer Institute, University of Minnesota, Minneapolis, Minnesota 55455, USA

‡mohammad.alidoust@ntnu.no; also at Department of Physics, Faculty of Sciences, University of Isfahan, Hezar Jerib Ave, Isfahan 81746-73441, Iran

[1] K. S. Novoselov *et al.*, Science **306**, 666 (2004); Y. Zhang *et al.*, Nature (London) **438**, 201 (2005); Y. W. Tan *et al.*, Eur. Phys. J. Spec. Top. **148**, 15 (2007).

[2] K. S. Novoselov *et al.*, Nature (London) **438**, 197 (2005).

[3] X. Du, I. Skachko, A. Barker, and E. Y. Andrei, Nat. Nanotech. **3**, 491 (2008).

[4] S. Das Sarma, S. Adam, E. H. Hwang, and E. Rossi, Rev. Mod. Phys. **83**, 407 (2011).

[5] A. H. Castro Neto *et al.*, Rev. Mod. Phys. **81**, 109 (2009).

[6] D. S. L. Abergel, V. Apalkov, J. Berashevich, K. Ziegler, and Tapash Chakraborty, Adv. Phys. **59**, 261 (2010).

[7] R. R. da Silva, J. H. S. Torres, and Y. Kopelevich, Phys. Rev. Lett. **87**, 147001 (2001).

[8] H. B. Heersche *et al.*, Nature (London) **446**, 56 (2007).

[9] X. Du, I. Skachko, and E. Y. Andrei, Phys. Rev. B **77**, 184507 (2008).

[10] P. Jarillo-Herrero *et al.*, Nature (London) **439**, 953 (2006).

[11] A. Shailos, W. Nativel, A. Kasumov, C. Collet, M. Ferrier, S. Gùeron, R. Deblock, and H. Bouchiat, Europhys. Lett. **79**, 57008 (2007).

[12] C. W. J. Beenakker, Rev. Mod. Phys. **80**, 1337 (2008).

[13] S. Bhattacharjee and K. Sengupta, Phys. Rev. Lett. **97**, 217001 (2006).

[14] G. Deutscher and P. G. De Gennes, *Superconductivity* (Dekker, New York, 1969).

[15] P. Burset, W. Herrera, and A. Levy Yeyati, Phys. Rev. B **80**, 041402(R) (2009).

[16] C. W. J. Beenakker, Phys. Rev. Lett. **97**, 067007 (2006).

[17] L. A. Ponomarenko, F. Schedin, M. I. Katsnelson, R. Yang, E. W. Hill, K. S. Novoselov, and A. K. Geim, Science **320**, 356 (2008).

[18] M. Titov and C. W. J. Beenakker, Phys. Rev. B **74**, 041401(R) (2006).

[19] J. P. Heida, B. J. van Wees, T. M. Klapwijk, and G. Borghs, Phys. Rev. B **60**, 13135 (1999).

[20] B. K. Nikolic, J. K. Freericks, and P. Miller, Phys. Rev. B **64**, 212507 (2001).

[21] I. Hagymàsi, A. Kormànyos, and J. Cserti, Phys. Rev. B **82**, 134516 (2010).

[22] M. Titov, A. Ossipov, and C. W. J. Beenakker, Phys. Rev. B **75**, 045417 (2007).

[23]P. Burset, A. Levy Yeyati, and A. Martin-Rodero, Phys. Rev. B **77**, 205425 (2008).
[24]C. H. Ahn *et al*., Rev. Mod. Phys. **78**, 1185 (2006).
[25]A. M. Black-Schaffer and S. Doniach, Phys. Rev. B **78**, 024504 (2008).
[26]J. Linder, A. M. Black-Schaffer, T. Yokoyama, S. Doniach, and A. Sudbø, Phys. Rev. B **80**, 094522 (2009).
[27]A. M. Black-Schaffer and J. Linder, Phys. Rev. B **82**, 184522 (2010).
[28]K. Halterman and O. T. Valls, Phys. Rev. B **65**, 014509 (2001).
[29]K. Halterman and O. T. Valls, Phys. Rev. B **69**, 014517 (2004).
[30]K. Halterman and O. T. Valls, Phys. Rev. B **72**, 060514 (2005).
[31]P. H. Barsic, O. T. Valls, and K. Halterman, Phys. Rev. B **75**, 104502 (2007).
[32]N. B. Kopnin and E. B. Sonin, Phys. Rev. Lett. **100**, 246808 (2008).
[33]P. B. Allen and R. C. Dynes, Phys. Rev. B **12**, 905 (1975).
[34]K. Levin and O. T. Valls, Phys. Rev. B **17**, 191 (1978).
[35]D. S. Falk, Phys. Rev. **132**, 1576 (1963).
[36]P. G. de Gennes, *Superconductivity of Metals and Alloys* (Addison-Wesley, Reading, MA, 1989).
[37]R. Saito, G. Dresselhaus, and M. S. Dresselhaus, *Physical Properties of Carbon Nanotubes* (Imperial College, London, 1998).
[38]S. Pilgram, W. Belzig, and C. Bruder, Phys. Rev. B **62**, 12462 (2000).
[39]D. Saint-James, J. Phys. (France) **25**, 899 (1964); A. F. Andreev, Sov. Phys. JETP **19**, 228 (1964).
[40]J. Cserti, I. Hagymási, and A. Kormányos, Phys. Rev. B **80**, 073404 (2009).
[41]A. Melsen, P. W. Brouwer, K. M. Frahm, and C. W. J. Beenakker, Europhys. Lett. **35**, 7 (1996).
[42]K. Halterman and O. T. Valls, Physica C **397**, 151 (2003).
[43]Y. J. Shin *et al*., Appl. Phys. Lett. **97**, 262105 (2010).
[44]J. Linder, A. M. Black-Schaffer, and A. Sudbø, Phys. Rev. B **82**, 041409(R) (2010).